PHYSICAL REVIEW B **72**, 161310(R) (2005)

Radius-dependent polarization anisotropy in semiconductor nanowires

A. V. Maslov and C. Z. Ning
Center for Nanotechnology, NASA Ames Research Center, Mail Stop 229-1, Moffett Field, California 94035, USA
(Received 12 May 2005; revised manuscript received 25 July 2005; published 24 October 2005)

Polarization anisotropy in semiconductor nanowires is studied using the standard eight-band $\mathbf{k}\cdot\mathbf{p}$ theory. We show that the anisotropy ratio ranges from giant (~90%) to moderate (~60%) for the nanowire radius between 3 and 10 nm. Our result resolves an apparent contradiction between a recent tight-binding study [M. P. Persson and H. Q. Xu, Phys. Rev. B **70**, 161310(R) (2004)], which predicts 100% anisotropy, and an earlier $\mathbf{k}\cdot\mathbf{p}$ study [P. C. Sercel and K. J. Vahala, Phys. Rev. B **44**, 5681 (1991)], which predicts 60% anisotropy independent of radius. We show that with proper inclusion of band mixing, the $\mathbf{k}\cdot\mathbf{p}$ theory agrees well with the tight-binding study on anisotropy.

DOI: 10.1103/PhysRevB.72.161310 PACS number(s): 73.21.Hb, 78.67.Lt

Chemical synthesis of free-standing semiconductor nanowires allows us to circumvent many technological difficulties encountered in the growth of heterostructure-based quantum wires and yields wires with well-controlled length, cross section, and location.[1] A particular interesting feature of a nanowire is polarization anisotropy of band-edge absorption, i.e., the difference in absorption properties depending whether the optical field is polarized along the nanowire or perpendicular to it. In thick nanowires, the polarization anisotropy is mostly caused by dielectric screening of the transverse component of the electric field.[2] In thin nanowires, anisotropy can also arise due to quantization of states and therefore alteration of selection rules for optical transitions.

Recently, a giant anisotropy of the optical polarization was predicted in very thin InP nanowires on the basis of a tight-binding model.[3] It was shown that the optical absorption (or luminescent emission) will be 100% polarized along the nanowire. If one defines a polarization ratio $r=(I_{\parallel}-I_{\perp})/(I_{\parallel}+I_{\perp})$ of the intensities parallel ($I_{\parallel}$) and perpendicular ($I_{\perp}$) to the wire, this gives $r=1$. Such a high degree of polarization is in contrast to the results of a simple $\mathbf{k}\cdot\mathbf{p}$ model of Sercel and Vahala[4] which predicts a much more modest value of anisotropy, namely, $r=0.6$. However, the latter value was obtained by considering only the heavy and light hole couplings in a typical zinc-blende semiconductor such as GaAs. Furthermore, the used assumption of infinite barriers makes this polarization ratio independent of the radius of the nanowire. These apparently conflicting results led to a conclusion that $\mathbf{k}\cdot\mathbf{p}$ theory is incapable of predicting polarization anisotropy correctly in thin nanowires.[3] We believe that this discrepancy between the tight-binding and envelope function theories can be explained by including more than just heavy–light holes in the $\mathbf{k}\cdot\mathbf{p}$ theory. In this paper we study systematically the radius dependence of polarization anisotropy in nanowires. We show that if all the coupling between six valence subbands and two conduction bands is included, the polarization anisotropy increases with decreasing nanowire radius. Our result, thus, provides a natural connection between the two theories and removes the apparent contradictions between the two results. It is also important to realize that the presence of contradictions between the $\mathbf{k}\cdot\mathbf{p}$ and tight-binding approaches are not unique to nanowires and have been widely discussed with respect to quantum dots.[5,6]

We start with a brief outline of our theoretical approach. We consider a cylindrical nanowire of radius R and oriented along z, which is also our axis of quantization. The Hamiltonian for zinc-blende lattices (in the spherical approximation in which the Luttinger parameters $\gamma_2=\gamma_3$) commutes with the angular momentum operator. Therefore, we seek the wave function that can be characterized by the z components of the wave number k_z and angular momentum F_z:

$$\Psi_{k_z F_z}=\frac{e^{ik_z z}}{\sqrt{L}}\sum_{n=1}^{8}\frac{e^{iM_n\varphi}}{\sqrt{2\pi}}f_n(\rho)U_n, \tag{1}$$

where $U_n=|J,J_z\rangle$ are the Bloch functions of a zinc-blende semiconductor at the bandedge (characterized by the total angular momentum J and its projection J_z), $f_n(\rho)$ are the radial parts of the envelope, and M_n are the azimuthal quantum numbers. The numbers M_n are chosen in such a way that the sum of each M_n and the corresponding z component of the angular momentum of the Bloch state gives F_z. We use the standard basis set $\{U_n\}$ and the Hamiltonian for zinc-blende semiconductors (see, for example, Ref. 7).

To find the envelopes $f_n(\rho)$ and energies we solve the Schrödinger equation numerically by using finite differences on a nonuniform grid along the ρ direction, similar to a one-band model.[8] The envelopes are sampled at the grid points and the differential operators in the Hamiltonian, such as $k_+=-i(\partial_x+i\partial_y)=-i[\partial_\rho+(i/\rho)\partial_\varphi]$, are approximated using finite differences. After discretization we obtain an eigenvalue problem for a non-Hermitian $8N\times 8N$ matrix, with N the number of grid points, which is diagonalized numerically using LAPACK's subroutine ZGEEV. We typically used 16–24 points inside the nanowire and 6–8 outside. All eigenenergies are checked to have negligible imaginary parts.

In order to avoid numerical problems that lead to unphysical results, we made two assumptions. First, the nanowire is surrounded by a material with a large band gap. Second, the mass in the conduction band is completely determined by the coupling to the valence band. As for the former assumption, we take the barrier height 2.5 eV both for the conduction and valence bands. The envelopes in this buffer layer decay exponentially and are assumed to reach zero at the end of the buffer layer, i.e., $f_n=0$. This buffer is necessary to provide

physically realistic boundary conditions for the conduction and valence envelopes. Setting all components to zero at the nanowire boundary gives reasonable results when the conduction and valence bands are treated separately. If the bands are coupled, setting all envelopes to zero results in an extremely steep change in the envelopes near the boundary. Physically, such rapid spatial change implies the broad spatial spectrum of the envelopes, which extends to the regions far from the zone center where $\mathbf{k}\cdot\mathbf{p}$ theory breaks down. Using a buffer layer with large but finite height, one obtains finite values for the envelopes at the boundary and smooth exponential decay in the buffer layer; the electrons are still confined inside the wire and no probability current exists at the boundary. We also use the same Luttinger parameters for the buffer as for the wire. This numerical procedure seems to be equivalent to using special boundary conditions separately for the valence- and conduction-band envelopes in which the envelopes do not vanish at the boundary.[9]

With respect to the neglect of the dispersion of the uncoupled conduction band, this requires a slight modification of the Kane energy E_P to fit the experimentally measured electron mass and was suggested by Foreman.[10] This procedure helps to avoid the so-called spurious solutions that appear because of a weak negative curvature of the conduction band in the absence of valence-conduction band coupling.

We also mention that the analytical solution for one band can be extended to include mixing in the valence band as described in Refs. 4, 7, and 11. In this approach, first, one seeks for the envelopes which are eigenfunctions of the two operators at the same time: of the projection of the total angular momentum on the z axis and of the Hamiltonian. One obtains that each component $f_n(\rho)$ is a Bessel function taken with some constant coefficient. Second, one forms a superposition of these eigenfunctions to satisfy the boundary conditions and obtains a transcendental equation whose solutions give the quantized energies. This approach becomes very cumbersome even for more than four bands and that is why we applied numerical discretization that seem to be easier when the coupling of many bands is required.

Our numerical results were obtained using the following material parameters for InP:[12] $E_g=1423.6$ meV ($T=0$ K), $m_c/m=0.0795$, $\gamma_1=5.08$, $\gamma_2=1.6$, $\gamma_3=2.10$. $\Delta_{\mathrm{so}}=108$ meV; all notations are standard. Adopting the spherical approximation we take $\gamma_{2,3}^{sp}=(2\gamma_2+3\gamma_3)/5=1.9$. Then we calculate the Kane energy using

$$E_P=\frac{m}{m_c}\left[\frac{2}{3E_g}+\frac{1}{3(E_g+\Delta_{\mathrm{so}})}\right]^{-1}=18337.9\ \mathrm{meV} \qquad (2)$$

which differs only by 11% from the actual value $E_p=20.700$ eV.[12]

Figure 1 shows the dispersion for the conduction and valence subbands with different quantum number F_z. For the conduction band, we see a rather significant deviation from the result of one-band model with the effective mass given at the zone center. Moreover, by using the one-band model one obtains the position of the lowest state at about 308 meV above the bulk energy. The eight-band model gives substantially smaller number, 183 meV. This discrepancy can be attributed to large quantization energies away from the conduction-band bottom where band mixing plays an essential role. We also verified that our results do not significantly change if we increase the height of the surrounding buffer layer.

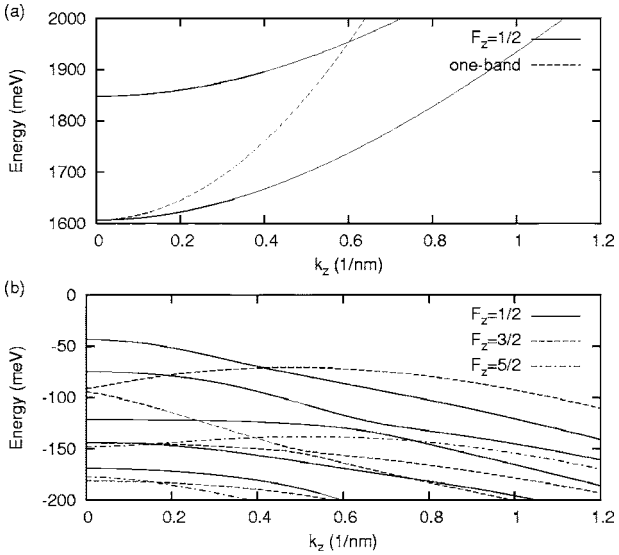

FIG. 1. Dispersion of conduction (a) and valence (b) subbands for a $R=3$ nm InP nanowire. In (a), the dashed line shows the parabolic dispersion that follows from a one-band model with the same quantization energy as the lowest state.

The structure of valence band is rather complicated with many crossings and anticrossings present [see Fig. 1(b)]. The states are usually mixtures of all Bloch components even at the zone center.[7,11,13] It is worth noting that the top state in the $F_z=\frac{3}{2}$ subspace has negative curvature and becomes higher in energy than the top state in the $F_z=\frac{3}{2}$ subspace at some finite k_z.

Let us discuss in detail the properties of the top state at $k_z=0$ in the valence band, as it determines the band-edge optical absorption. The state is neither a heavy hole nor light hole, as pointed out by several authors.[4,7,11,13] This state is double degenerate with $F_z=\pm\frac{1}{2}$. To be specific, we discuss the state with $F_z=\frac{1}{2}$; the other state has the same properties. The state with $F_z=\frac{1}{2}$ is formed by superimposing the light- and heavy-hole states with $F_z=\frac{1}{2}$.[4,7,11] These holes are mixtures of the $|3/2,1/2\rangle$ and $|3/2,-3/2\rangle$ components because the holes move perpendicular to z. Using the analytical technique of Ref. 7, keeping only four valence subbands, and assuming infinite barriers, we obtain that the lowest state is about 60% light hole and 40% heavy hole in character. However, the supersposition of light- and heavy-holes states, needed to match the boundary conditions, gives a wave function that has 98% contribution from the $|3/2,1/2\rangle$ component. The contributions of the $|3/2,-3/2\rangle$ components from the light and heavy holes interfere most destructively. This result allows one to use a simple quantization rule for the top state: the state is formed by the $|3/2,1/2\rangle$ component and its energy is quantized as if it has the transverse mass $m/(\gamma_1-\gamma_2)$, which comes from the diagonal element of the Hamiltonian. This gives the quantized energy $E=-\hbar^2(\gamma_1-\gamma_2)k^2/$

$(2m)$, where k is determined by the first root of $J_0(kR)=0$ with J_0 the Bessel function of the first kind. We emphasize here again that the factor $\gamma_1-\gamma_2$ does not enter into the bulk light or heavy-hole masses. Thus, the resultant state is, strictly speaking, neither heavy nor light hole. This fact is often neglected in one-band models.[14] The approximate dispersion equation is much simpler than the exact one.[4,7,11] The precision is rather high. For example, keeping only heavy and light holes, assuming infinitely high boundaries and material parameters of InP, we obtain the exact energy $E=-18.3$ meV and approximate one $E=-19.5$ meV for a $R=6$ nm nanowire. The error is only 6.6%.

The optical absorption can be directly calculated using Maxwell's equations using the optical current **J** induced by an optical field with amplitude **E**:

$$J_x = \delta(x)\delta(y)\sigma_x E_x, \tag{3}$$

where the δ functions imply the smallness of the nanowire radius in comparison to the wavelength. The subscript x denotes orientation and a similar expression exists for J_z. Calculating the optical current by using the Schrödinger equation with field-wire interaction in the dipole approximation, we obtain

$$\sigma_x(\omega) = \left. \frac{e^2P^2}{\hbar^2\omega}\frac{|\tilde{P}_x|^2}{|\partial_{k_z}E_{k_z}|}\right|_{E_{k_z}=\hbar\omega}, \tag{4}$$

where $P=\sqrt{E_P\hbar^2/2m}$.[15] The dimensionless momentum matrix element is

$$\tilde{P}_x = \sum_{n,m}\tilde{p}_x^{nm}\delta_{M_n,M_m}\int_0^R \rho\, d\rho\, f_n^*(\rho)f_m(\rho), \tag{5}$$

where $\tilde{p}_x^{nm}$ is the dimensionless momentum matrix element between two Bloch states with indices m and n. Expressions similar to (4) and (5) exist for σ_z.

Figure 2 shows the transverse (σ_x) and longitudinal (σ_z) components of the optical conductivity for nanowires with radii $R=3$, 6, and 10 nm. The left frames show the conductivities calculated according to Eq. (4); the right frames show the conductivities which were convoluted with a 1 meV wide Lorentzian. Comparing the results for $R=3$ nm and $R=6$ nm we clearly see that the longitudinal component becomes more dominant as the radius of the nanowire decreases. The same trend holds if we include the data for a $R=10$ nm nanowire. However, for the $R=10$ nm nanowire the quantization in the valence band becomes rather weak and several transitions are very close to the band edge. For such a thick nanowire, making the Lorentzian broadening larger will significantly reduce polarization anisotropy.

To evaluate the polarization anisotropy we compute

$$r = \frac{|\tilde{P}_z|^2 - |\tilde{P}_x|^2}{|\tilde{P}_z|^2 + |\tilde{P}_x|^2} \tag{6}$$

at the zone center since the matrix elements determine the heights of the absorption peaks. This ratio is plotted in Fig. 3 for InP and GaAs using various models. In the six-band model, we decoupled the conduction band and assumed infinite barriers. In the four-band model, we further decoupled the split-off states. The results of six- and four-band models do not change significantly if we take barrier height 2.5 eV rather than infinity. However, both these models will give a much higher quantization energy in the conduction band. The anisotropy ratio for InP is around 0.66 at $R=10$ nm and becomes 0.88 at $R=3$ nm in the eight-band model. However, even a six-band model gives a monotonic increase of polarization anisotropy with decreasing radius. The four-band model shows essentially a radius-independent behavior. This difference in behaviors can be readily explained. In the four-band model, all Hamiltonian terms are proportional to wave

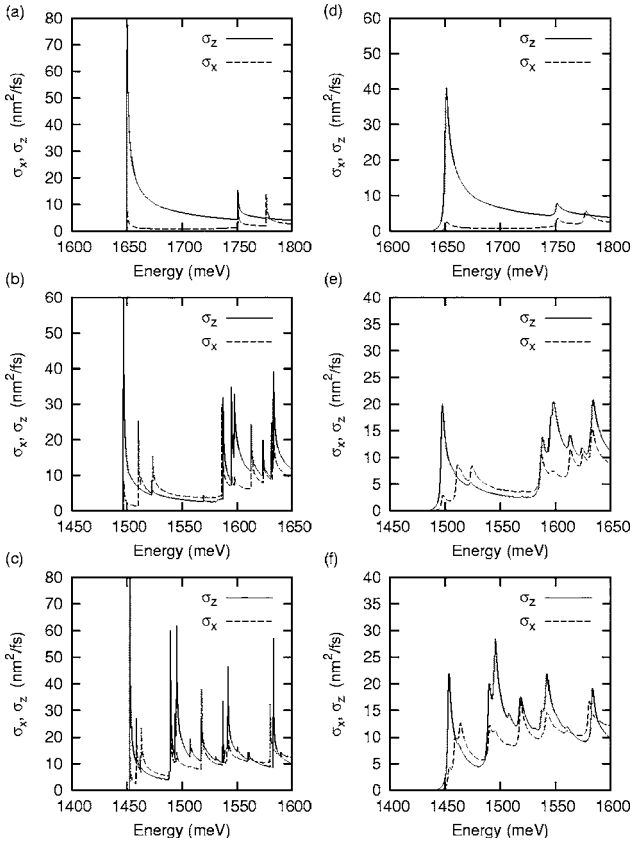

FIG. 2. Optical conductivities σ_x and σ_z for (a) $R=3$ nm, (b) $R=6$ nm, and (c) $R=10$ nm nanowires. (d), (e), and (f) show the same conductivities as in (a), (b), (c), respectively, but convoluted with a 1 meV wide Lorentzian.

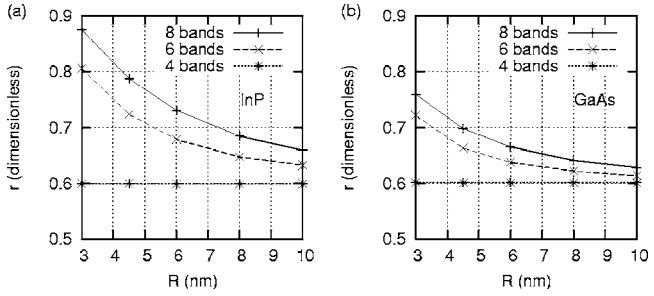

FIG. 3. Polarization anisotropy ratio r as a function of R for (a) InP and (b) GaAs calculated using eight-, six-, and four-band models.

numbers (or derivatives). Thus, the shapes of all bands are essentially independent of radius. However, the split-off terms contain the split-off energy Δ_{so} which breaks the scalability of band structure with radius. In other words, the band-edge properties of nanowires of different radii are no longer related in a simple manner. Moreover, the contribution of the split-off states to the top valence subband increases with decreasing radius as the top state is pushed down closer to the split-off energy. This effect in InP is larger than in GaAs due to much smaller split-off energy, 108 meV for InP vs 341 meV for GaAs (see Fig. 3). Additional coupling to the conduction band, makes the anisotropy ratio even bigger compared to the six-band model. For the smallest nanowire we considered, $R=3$ nm, our polarization anisotropy is still smaller than $r=1$, predicted using a tight-binding model.[3] The discrepancy may be partly due to different nanowire cross sections: circular in our model and hexagonal in the model of Ref. 3. However, we can clearly see the general tendency of anisotropy increase with decreasing radius.

To explain qualitatively the change in polarization anisotropy with radius, we take the $|3/2,1/2\rangle$ component, which dominates in the top valence state as we showed earlier, and couple it to the split-off component $|1/2,1/2\rangle$. The explicite expressions for these two basis functions are

$$|3/2,1/2\rangle = \sqrt{\frac{1}{3}}\left(-\frac{|x\rangle + i|y\rangle}{\sqrt{2}}\right)|\downarrow\rangle + \sqrt{\frac{2}{3}}|z\rangle|\uparrow\rangle,$$

$$|1/2,1/2\rangle = \sqrt{\frac{2}{3}}\left(-\frac{|x\rangle + i|y\rangle}{\sqrt{2}}\right)|\downarrow\rangle - \sqrt{\frac{1}{3}}|z\rangle|\uparrow\rangle. \quad (7)$$

The Hamiltonian in this subspace is

$$H = -\frac{\hbar^2}{2m}\begin{pmatrix} (\gamma_1-\gamma_2)\hat{k}_\perp^2 & \gamma_2\hat{k}_\perp^2/\sqrt{2} \\ \gamma_2\hat{k}_\perp^2/\sqrt{2} & 2m\Delta_{so}/\hbar^2 + \gamma_1\hat{k}_\perp^2 \end{pmatrix}, \quad (8)$$

where $\hat{k}_\perp$ is the transverse momentum operator. We seek a φ-independent eigenstate of (8) in the form

$$\Psi = (A|3/2,1/2\rangle + B|1/2,1/2\rangle)J_0(k\rho), \quad (9)$$

where A and B are constant coefficients. Diagonalization gives two branches for $E(k)$. To find quantized states we need to form a superposition of the two eigenstates and impose boundary conditions. However, since the state (9) has a common $J_0(k\rho)$ dependence, each of the eigenstates can satisfy the boundary condition $J_0(k(E)R)=0$ independently. Thus, we take the branch which has the highest energy and calculate A and B (see Fig. 4). As the quantized k increases (R decreases) the coefficient B becomes negative and increases in magnitude, while A slightly decreases. Substituting (7) into (9), we observe that the weights of the $|x\rangle$ and $|y\rangle$ components decrease while that for $|z\rangle$ increases. Considering the optical transitions to the lowest state in the conduction band, the absorption for the z polarized light increases in comparison the x or y polarized light. For large R (small k) we have polarization anisotropy (given only by the $|3/2,1/2\rangle$ state) $r=(2/3-1/6)/(2/3+1/6)=60\%$. Thus, the change of anisotropy can be explained by the presence of the split-off states.

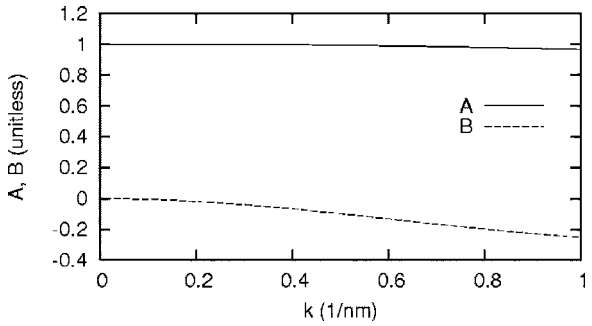

FIG. 4. Coefficients A and B as functions of k.

To conclude, using numerical modeling and a simple analytical theory we showed that both six- and eight-band $\mathbf{k}\cdot\mathbf{p}$ models predict a monotonic increase in polarization anisotropy with decreasing radius in InP nanowires. Our results provide a smooth transition and explains the discrepancies between two regimes: that of moderately thin quantum wires, in which only the heavy and light holes are sufficient to describe the band-edge properties,[4] and that of extremely thin nanowires, for which a tight-binding model has been applied.[3]

The work of A.V.M. was supported by a NASA grant to ELORET Corp. (Sunnyvale, California, USA).

[1] For a review, see Adv. Mater. **15** (5) (2005), Special Issue: Nanowires.
[2] J. Wang, M. S. Gudiksen, X. Duan, Y. Cui, and C. M. Lieber, Science **293**, 1455 (2001).
[3] M. P. Persson and H. Q. Xu, Phys. Rev. B **70** 161310(R) (2004).
[4] P. C. Sercel and K. J. Vahala, Phys. Rev. B **44**, 5681 (1991).
[5] O. Stier, R. Heitz, A. Schliwa, and D. Bimberg, Phys. Status Solidi A **190**, 477 (2002).
[6] H. Fu, L. W. Wang, and A. Zunger, Appl. Phys. Lett. **71**, 3433 (1997); **73**, 1157 (1998); Al. L. Efros and M. Rosen, *ibid.* **73**, 1155 (1998).
[7] P. C. Sercel and K. J. Vahala, Phys. Rev. B **42**, 3690 (1990).
[8] A. V. Kuznetsov, G. D. Sanders, and C. J. Stanton, Phys. Rev. B **52**, 12 045 (1995).
[9] A. V. Rodina, A. Yu. Alekseev, Al. L. Efros, M. Rosen, and B. K. Meyer, Phys. Rev. B **65**, 125302 (2002).
[10] B. A. Foreman, Phys. Rev. B **56**, R12748 (1997).
[11] M. Sweeny, J. Xu, and M. Shur, Superlattices Microstruct. **4**, 623 (1988).
[12] I. Vurgaftman, J. R. Meyer, and L. R. Ram-Mohan, J. Appl. Phys. **89**, 5815 (2001).
[13] D. S. Citrin and Y. C. Chang, Phys. Rev. B **40**, 5507 (1989).
[14] S. Glutsch and D. S. Chemla, Phys. Rev. B **53**, 15902 (1996); A. N. Forshaw and D. M. Whittaker, Phys. Rev. B **54**, 8794 (1996).
[15] A. V. Maslov and C. Z. Ning, Phys. Rev. B **72**, 125319 (2005).